

Journal Pre-proof

Th⁴⁺ tuned aggregation-induced emission: A novel strategy for sequential ultrasensitive detection and separation of Th⁴⁺ and Hg²⁺

You-Ming Zhang, Wei Zhu, Qi Zhao, Wen-Juan Qu, Hong Yao, Tai-Bao Wei, Qi Lin



PII: S1386-1425(19)31317-4

DOI: <https://doi.org/10.1016/j.saa.2019.117926>

Reference: SAA 117926

To appear in: *Spectrochimica Acta Part A: Molecular and Biomolecular Spectroscopy*

Received date: 16 August 2019

Revised date: 21 November 2019

Accepted date: 6 December 2019

Please cite this article as: Y.-M. Zhang, W. Zhu, Q. Zhao, et al., Th⁴⁺ tuned aggregation-induced emission: A novel strategy for sequential ultrasensitive detection and separation of Th⁴⁺ and Hg²⁺, *Spectrochimica Acta Part A: Molecular and Biomolecular Spectroscopy*(2019), <https://doi.org/10.1016/j.saa.2019.117926>

This is a PDF file of an article that has undergone enhancements after acceptance, such as the addition of a cover page and metadata, and formatting for readability, but it is not yet the definitive version of record. This version will undergo additional copyediting, typesetting and review before it is published in its final form, but we are providing this version to give early visibility of the article. Please note that, during the production process, errors may be discovered which could affect the content, and all legal disclaimers that apply to the journal pertain.

© 2019 Published by Elsevier.

Th⁴⁺ tuned aggregation-induced emission: a novel strategy for sequential ultrasensitive detection and separation of Th⁴⁺ and Hg²⁺

You-Ming Zhang^{a,b,*}, Wei Zhu^b, Qi Zhao^b, Wen-Juan Qu^b, Hong Yao^b, Tai-Bao Wei^b, Qi Lin^{b,*}

^a College of Chemistry and Chemical Engineering, Lanzhou City University, Lanzhou, Gansu, 730070, P. R. China. E-mail: zhangnwnu@126.com.

^b Research Center of Gansu Military and Civilian Integration Advanced Structural Materials, College of Chemistry and Chemical Engineering, Northwest Normal University, Lanzhou, Gansu, 730070, P. R. China. E-mail: linqi2004@126.com.

Abstract

A novel strategy, Th⁴⁺ tuned aggregation-induced emission, for sequential ultrasensitive detection and separation of Th⁴⁺ and Hg²⁺ was developed successfully. For demonstration this strategy, we designed and synthesized two tripodal gelators **TH** (tri-(isoniazid-4-yl)-functionalized trimesic acylhydrazine) and **TA** (tri-(pyridine-4-yl)-functionalized trimesic amide). The **TH** and **TA** could assemble into a stable supramolecular polymer hydrogel **THTA-G** in DMSO/H₂O (3.3:6.7, v/v) binary-solution. The **THTA-G** does not show aggregation-induced emission (AIE) effect. However, after addition of Th⁴⁺ into the **THTA-G**, the obtained metallogel **THTA-GTh** shows strong green AIE effect, which indicated that Th⁴⁺ could tune the gel generation of AIE effect. Interestingly, the **THTA-G** could ultrasensitive fluorescently detect Th⁴⁺, and the corresponding metallogel **THTA-GTh** could ultrasensitively detect Hg²⁺. The detection limits of **THTA-G** and **THTA-GTh** for Th⁴⁺ and Hg²⁺ are 8.61×10^{-11} mol/L and 1.08×10^{-11} mol/L, respectively. Additionally, the xerogels of **THTA-G** and **THTA-GTh** could separate Th⁴⁺ and Hg²⁺ from aqueous solution with excellent ingestion capacity, and the **THTA-G** could be used as a writable smart light-emitting material.

Keywords: Ultrasensitive, Detection and separation, Aggregation-induced emission; Supramolecular polymer hydrogel, Smart light-emitting material

1. Introduction

In recent years, ultrasensitive detection has attracted much attention due to the development of ultrasensitive strategies for detecting specific analytes is crucial for biological samples and environmental safety [1-3]. To date, some strategies have been reported for detect ultralow concentrations of heavy metal ions. For example, Quan et al. reported a ratiometric fluorescence sensor for ultrasensitive detection of Cu^{2+} ion by a cation-exchange strategy [4]. Nandi et al. synthesized a nitrogen doped PEGylated carbon dots (C-dots) for ultrasensitive detection of Hg^{2+} ion [5]. However, these strategies suffer from several drawbacks that include high-cost, sophisticated procedures, and lack of portability [6,7]. Therefore, exploring novel strategies for efficient ultrasensitive detection of important analytes is great urgently needed.

As we all know, Thorium (typical as Th^{4+}) is an important radioactive element in nuclear safeguards due to its broad applications in many nuclear industries. However, the presence of Th^{4+} in the environment is an important concern due to its toxicity and health effects on human body [8,9]. In addition, Hg^{2+} can readily penetrate through biological membranes and cause severe damage to the brain, heart, kidneys and nervous system [10,11]. All of the above reasons promote urgent research on Th^{4+} and Hg^{2+} ultrasensitive detection and separation from environmental.

In 2001, Tang's group [12] pioneered the concept of aggregation-induced emission (AIE), which is essentially the opposite effect to notorious aggregation-caused quenching (ACQ) [13]. Enhanced emission is attributed to the synergetic effect of aggregation-induced planarization and J-type aggregate formation, which help to prevent intramolecular rotations [14,15]. Since this pioneering work, a series of interesting molecules with AIE effect have been studied and used as chemosensors, stimuli-responsive nanomaterials, organic light-emitting diodes, etc [16-18]. It is worth noting that the development of AIE also provide a new platform for ultrasensitive detection.

Smart supramolecular polymer hydrogels are an important subclass in the area of supramolecular polymers [19,20], which can be constructed from gelators assembling through the driving force of multiple non-covalent interactions (H $\cdots\pi$, H \cdots H, O \cdots H, and N \cdots H) and weak intermolecular face-to-face π - π interactions in appropriate solvent systems [21-24]. Nowadays, supramolecular polymer hydrogels have been widely applied in chemosensors, biomaterials, pollutant removal, drug delivery and light-harvesting system due to their unique structures and fantastic properties [25-29]. However, smart supramolecular polymer hydrogels based on two tripodal gelators, which can carry out sequential ultrasensitive detection and separation of Th $^{4+}$ and Hg $^{2+}$ are never been reported.

Inspired by this fact and as a part of our research effort [30-32], herein, we reported a novel strategy, Th $^{4+}$ tuned aggregation-induced emission, for sequential ultrasensitive detection and separation of Th $^{4+}$ and Hg $^{2+}$. First, two tripodal gelators **TH** (tri-(isoniazid-4-yl)-functionalized trimesic acylhydrazine) and **TA** (tri-(pyridine-4-yl)-functionalized trimesic amide) were designed and successfully prepared. The two gelators contain multiple hydrogen-bonding sites (acylhydrazine and amide groups), which might be great use in the supramolecular self-aggregation process. Meanwhile, multiple coordination sites for metal ions also give the two gelators second driving force for assembly through the strong coordination interactions between metal ions and acylhydrazine and amide groups.

Indeed, the **TH** (host) and **TA** (guest) could assemble into a stable supramolecular polymer hydrogel **THTA-G** with weak fluorescence in a mixed solvent of DMSO/H $_2$ O (3.3:6.7, v/v). Intriguingly, after addition of Th $^{4+}$ into the **THTA-G**, the obtained metallogel **THTA-GTh** showed strong green AIE effect. These results indicated that Th $^{4+}$ could restriction of intramolecular rotation (RIR), and then tune the gel generation of AIE effect. Additionally, Hg $^{2+}$ could induce the fluorescence of **THTA-GTh** to weaken again by cation- π interactions. Therefore, Th $^{4+}$ tuned aggregation-induced emission is a simple and efficient novel strategy for sequential ultrasensitive detection of Th $^{4+}$ (LOD = 8.61×10^{-11} mol/L) and Hg $^{2+}$ (LOD = 1.08×10^{-11} mol/L). Significantly, the xerogels of **THTA-G** and **THTA-GTh** could

separation of Th⁴⁺ and Hg²⁺ from aqueous solution with nice adsorption property, respectively. More importantly, the **THTA-G** could act as a novel smart light-emitting material.

2. Experiment section

2.1. Materials and instruments

All starting materials were obtained from commercial supplies and used as received. All cations (Table S1) were made into aqueous solution ($c = 0.1 \text{ mol/L}$). ¹H NMR spectra were recorded on Mercury-600 BB spectrometer at 600 MHz and Mercury-400 BB spectrometer at 400 MHz. ¹³C NMR spectra were recorded on Mercury-600 BB spectrometer at 151 MHz. High-resolution mass spectra were performed on Bruker Esquire 3000 plus mass spectrometer equipped with ESI interface and ion trap analyzer. Fluorescence spectra were performed on Shimadzu RF-5301PC fluorescence spectrophotometer. Infrared spectra were performed on Digilab FTS-3000 FTIR spectrophotometer and X-ray diffraction (XRD) pattern was tested using Rigaku RINT2000 diffract meter equipped (copper target; $\lambda = 0.154073 \text{ nm}$). Scanning electron microscopy (SEM) images of the xerogels were investigated using JSM-6701F instrument at an accelerating voltage of 8 kV. Transmission electron microscope (TEM) images of the xerogels were obtained on FEI Tecna G2 F20 apparatus operating at 200 KV. Fluorescent information of the gels was characterized using Laser Scanning Confocal Microscope (LSCM, Olympus Fluoview FV1200).

Scheme 1

2.2. Synthesis and characterization of **TA**.

Dissolving the 1,3,5-benzenetricarbonyl trichloride (0.2655 g, 1.0 mmol) with DMF (10 mL), then the solution was dropwise added to a mixture of 4-aminopyridine (0.3106 g, 3.3 mmol) and TEA (1 mL) in DMF (20 mL). The reaction mixture was stirred at room temperature for 24 h. Recrystallization of **TA** after the reaction was completed, and then dried under vacuum. Yield: 90% (0.3943g). M.p.: 270~272 °C. ¹H NMR (400 MHz, DMSO-*d*₆), δ/ppm : 10.98 (s, 3H), 8.79-8.75 (t, $J = 8.6 \text{ Hz}$, 3H), 8.55-8.52 (t, $J = 5.4 \text{ Hz}$, 6H), 7.84-7.82 (t, $J = 4.4 \text{ Hz}$, 6H). ¹³C NMR (151 MHz, DMSO-*d*₆), δ/ppm : 166.05, 165.66, 150.87, 150.78, 146.26, 146.13, 145.41, 135.38,

134.92, 132.15, 131.03, 114.60, 109.24. HRMS: m/z [**TA** + H]⁺ calcd for C₂₄H₁₉N₆O₃, 439.1519; found 439.1515.

2.3. Synthesis and characterization of **TH**.

Dissolution of 1,3,5-benzenetricarbonyl trichloride (0.2655 g, 1.0 mmol) with CH₂Cl₂ (10 mL), then the solution was dropwise added to a solution of isoniazid (0.4526 g, 3.3 mmol) in CH₂Cl₂ (20 mL). After the reaction mixture was stirred at room temperature for 24 h, the **TH** was filtrated and then dried under vacuum. Yield: 92% (0.5521g). M.p.: 167 ~ 169 °C. ¹H NMR (400 MHz, DMSO-*d*₆), δ/ppm: 11.03-11.01 (d, *J* = 10.4 Hz, 6H), 8.74-8.73 (m, 9H), 7.78-7.77 (m, 6H). ¹³C NMR (151 MHz, DMSO-*d*₆), δ/ppm: 165.16, 164.55, 164.50, 150.64, 140.13, 138.94, 133.73, 130.37, 121.97, 121.91. HRMS: m/z [**TH** + Na]⁺ calcd for C₂₇H₂₂N₉O₆Na, 590.1512; found 590.1584.

2.4. Preparation of supramolecular polymer hydrogel **THTA-G**.

The **THTA-G** was prepared by addition of **TH** (0.01 g) and **TA** (0.0077 g) to the DMSO/H₂O (3.3:6.7, v/v) solution (300 μL) in a reagent bottle (1 mL), and then heated the mixture until the two gelators were dissolved completely. After the solution was cooled to room temperature, the supramolecular polymer hydrogel **THTA-G** formed. Qualitatively, gelation was considered successful if no sample flow was observed upon inversion of the container at 25 °C. Additionally, the xerogel was obtained by drying hydrogel **THTA-G** under reduced pressure.

2.5. Preparation of supramolecular polymer metallo gel **THTA-GTh**.

The gelators **TH** (0.01 g) and **TA** (0.0077 g) were put in a reagent bottle (1 mL), and the mixture of DMSO/H₂O (3.3:6.7, v/v) solution (300 μL) were also added to the reagent bottle as solvents. Then, the aqueous solution of Th⁴⁺ (0.65 μL, 0.1 mol/L) was added to the mixture. After that, the mixture was heated until the solid were dissolved completely, then cooled it to room temperature, the supramolecular polymer metallo gel **THTA-GTh** will be obtained. Additionally, the xerogel was obtained by drying metallo gel **THTA-GTh** under reduced pressure.

2.6. The technical details for the measurement of fluorescence spectra of gel sample.

First, in order to investigate the fluorescence response properties of **THTA-G** to metal ions, various metal ions aqueous solution (Hg^{2+} , Fe^{3+} , Ag^+ , Zn^{2+} , Ca^{2+} , Ni^{2+} , Co^{2+} , Pb^{2+} , Cr^{3+} , Cu^{2+} , Mg^{2+} , Ba^{2+} , Cd^{2+} , Al^{3+} , Eu^{3+} , Tb^{3+} , La^{3+} and Th^{4+}) were added into **THTA-G** (3.3 wt%, 10 mg/ml = 1.0%), respectively. Any fluorescence changes of **THTA-G** after addition of different metal ions were recorded on a Shimadzu RF-5301PC fluorescence spectrometer. As a result, only upon the addition of Th^{4+} into **THTA-G**, the fluorescence emission of **THTA-G** could be enhanced and make the fluorescence become strong green. The obtained Th^{4+} coordinated metallogel is named as **THTA-GTh**.

Next, for **THTA-GTh**, in order to study the successive fluorescence response properties of **THTA-GTh** to metal ions, a series of metal ions aqueous solution such as Hg^{2+} , Fe^{3+} , Ag^+ , Zn^{2+} , Ca^{2+} , Ni^{2+} , Co^{2+} , Pb^{2+} , Cr^{3+} , Cu^{2+} , Mg^{2+} , Ba^{2+} , Cd^{2+} , Al^{3+} , Eu^{3+} , Tb^{3+} and La^{3+} were added into **THTA-GTh**, respectively. Then, we also use Shimadzu RF-5301PC spectrometer to record the changes in fluorescence of the metallogels. As a result, only Hg^{2+} could induce the fluorescence of **THTA-GTh** to weaken again.

Fig. 1.

3. Results and discussion

The gelators **TH** and **TA** were prepared via two simple routes (Scheme 1) and well characterized using ^1H NMR, ^{13}C NMR and HRMS techniques (Fig. S1-S6). The **TH** and **TA** could form a stable supramolecular polymer hydrogel **THTA-G** in a mixed solvent system of DMSO/ H_2O (3.3:6.7, v/v) (Fig. 1). The gelation concentration of **THTA-G** is about 3.3 wt%, and gel-sol transition temperature (T_{gel}) is approximately 115 °C. The fluorescence intensity of **THTA-G** is very strong when the temperature is higher than T_{gel} . However, after the **THTA-G** formed, the fluorescence intensity decreased approximately by 2.7-fold and the emission maxima shifted from 470 to 485 nm (Fig. 2a). The laser scanning confocal microscopy (LSCM) experiments also demonstrated the **THTA-G** emitting weak fluorescence under ultraviolet light (Fig. 3a). This phenomenon of decreased fluorescence could be satisfactorily explained by a typical ACQ (aggregation-caused quenching) mechanism [33,34]. In this case, intermolecular hydrogen bond interactions or other non-radiative channels to form

excimer or excinlex consume the energy of excited state and cause a decrease in radiative emission.

Fig. 2.

Fig. 3.

The possible assembly mechanism of **TH** and **TA** was investigated via high-resolution mass spectrometry (HRMS), proton nuclear magnetic resonance spectroscopy (^1H NMR), two-dimensional NOESY nuclear magnetic resonance spectroscopy (2D NOESY NMR), fourier-transform infrared spectroscopy (FT-IR), X-ray diffraction (XRD), scanning electron microscopy (SEM) and transmission electron microscopy (TEM) analyses. In the HRMS of xerogel **THTA-G** (Fig. S7), a peak exhibited at $m/z = 1006.3138$ [**TH+TA+H**] $^+$, which confirmed the stoichiometry of **TH** and **TA** was 1:1. As shown in Fig. 4a, with the addition of **TA** to **TH**, the signals of protons H_a and H_b on **TH** shifted downfield, and H_c , H_d , H_e on **TH** shifted upfield. Meanwhile, the signals of protons H_1 , H_2 , H_3 and H_4 on **TA** shifted downfield. As the concentration of **TH** and **TA** increased (Fig. 4b), the signals of protons H_a and H_b on **TH** shifted downfield, while H_c , H_d and H_e shifted upfield. At the same time, the signals of protons H_1 , H_2 , H_3 and H_4 on **TA** shifted downfield. These results confirmed the existence of intermolecular interactions in the assemble process of **TH** and **TA**, and stable intermolecular hydrogen bonds also formed between N-H and C=O groups. Moreover, all the signal peaks became broad at high concentration, which illustrated the formation of supramolecular polymer driven by intermolecular interactions. The 2D NOESY NMR (Fig. S8) experiments displayed the correlation between signals of protons H_a , H_b , H_c , H_d , H_e and H_1 , H_2 , H_3 , H_4 , which also demonstrated the existence of intermolecular interactions between **TH** and **TA**.

Fig. 4.

According to the FT-IR spectra of **TH**, **TA** and **THTA-G** (Fig. S9a), for **THTA-G**, compared with **TH** (N-H: 3470 cm^{-1} , C=O: 1664 cm^{-1}) and **TA** (N-H: 3475 cm^{-1} , C=O: 1615 cm^{-1}), the stretching vibration peaks of N-H and C=O all became a broad peak and shifted to 3465 cm^{-1} and 1610 cm^{-1} , respectively, which also indicated that hydrogen bond interactions involved in the assemble process of **TH** and **TA**. In

addition, the assembly process of **TH** and **TA** was also investigated by the small-angle XRD pattern. As shown in Fig. S10a, there were many sharp peaks at 2θ from 20 to 30 degrees, indicating that **TH** and **TA** have long-range ordered structure in the xerogel state. However, there were only two sharp peaks at 2θ from 10 to 15 degrees in **THTA-G**, suggesting that π - π stacking interaction were not involved in the gelation process, and hydrogen bond interactions involved in the assemble process of **TH** and **TA** [35,36]. Importantly, the SEM images (Fig. S11) also supported above proposed assemble mechanism. The **TA** shows rod-like structure and **TH** shows amorphous structure. However, the xerogel of **THTA-G** shows tire-shaped structure with tightly stacking. Moreover, in TEM image of **THTA-G** (Fig. S12a), the distance between layer and layer of tire is about 72 nm. These results indicated that the **TA** and **TH** could assemble into supramolecular polymer hydrogel **THTA-G** in aqueous media by intermolecular interactions (Scheme 2a).

Scheme 2.

Fig. 5.

The metal ions response properties of **THTA-G** were investigated carefully by the addition of various metal ions aqueous solution including Hg^{2+} , Fe^{3+} , Ag^+ , Zn^{2+} , Ca^{2+} , Ni^{2+} , Co^{2+} , Pb^{2+} , Cr^{3+} , Cu^{2+} , Mg^{2+} , Ba^{2+} , Cd^{2+} , Al^{3+} , Eu^{3+} , Tb^{3+} , La^{3+} and Th^{4+} into the **THTA-G**, respectively. As a result, only Th^{4+} could enhance the fluorescence of **THTA-G** and make the fluorescence become strong green (Fig. 5a and 6a). The results suggested that **THTA-G** could selectively detect Th^{4+} . According to fluorescent titrations of **THTA-G** for Th^{4+} (Fig. 6c) and $3\delta/S$ method [37], the detection limit of **THTA-G** for Th^{4+} is 8.61×10^{-11} mol/L (Fig. 7a and S13). Moreover, the **THTA-G** shows good binding affinity with Th^{4+} with an association constant (K_a) of 7.14×10^4 mol/L (Fig. S14). Importantly, the LOD (limit of detection) of **THTA-G** for Th^{4+} is lower than some other reported fluorescent sensors for Th^{4+} (Table S2), which indicated that the **THTA-G** could carry out ultrasensitive and selective detection of Th^{4+} from aqueous solution. Meanwhile, in order to investigate the selectivity of **THTA-G** for Th^{4+} , the control experiments were carried out under

the competition conditions. The coexist competition cations could not induce any interfere for the Th^{4+} sensing process for **THTA-G** (Fig. S15).

Fig. 6.

Fig. 7.

One of the values mentioned is that the **THTA-G** could be tuned by Th^{4+} to form metallogel **THTA-GTh**. The fluorescence intensity of **THTA-GTh** is negligible when the temperature is higher than 95 °C. However, when the **THTA-GTh** formed, the fluorescence intensity increased approximately by 5.6-fold and the emission maxima shifted from 465 to 470 nm (Fig. 2b). The LSCM experiments also demonstrated the **THTA-GTh** emitting strong green fluorescence under ultraviolet light (Fig. 3b). This phenomenon of enhanced fluorescence could be explained by an amazing AIE mechanism [38,39]. In this case, Th^{4+} could restriction of intramolecular motions in the aggregation state, and then blocks the nonradiative decay of excited state species and opening up a radiative channel. Moreover, being influenced by the aggregation effect, the emission maximum of metallogel was found to be red shifted by 5 nm. Therefore, the strong green fluorescence is an aggregation-induced emission (AIE).

Then, the successive metal ions response properties of **THTA-GTh** were investigated by adding a series of metal ions aqueous solution such as Hg^{2+} , Fe^{3+} , Ag^+ , Zn^{2+} , Ca^{2+} , Ni^{2+} , Co^{2+} , Pb^{2+} , Cr^{3+} , Cu^{2+} , Mg^{2+} , Ba^{2+} , Cd^{2+} , Al^{3+} , Eu^{3+} , Tb^{3+} and La^{3+} into **THTA-GTh**, respectively. As a result, the **THTA-GTh** could selectively recognize Hg^{2+} obviously (Fig. 5b). The LSCM experiment demonstrated the complex of **THTA-GTh** and Hg^{2+} also emitting weak fluorescence under ultraviolet light (Fig. 3c). According to fluorescent titrations of **THTA-GTh** for Hg^{2+} (Fig. 6d) and 3 δ /S method, the LOD of **THTA-GTh** for Hg^{2+} is 1.08×10^{-11} mol/L (Fig. 7b and Fig. S16). Importantly, the LOD of **THTA-GTh** for Hg^{2+} is also lower than some other reported fluorescent sensors for Hg^{2+} (Table S3). Thus, the **THTA-GTh** is capable of ultrasensitive and selective detection of Hg^{2+} from aqueous solution. Meanwhile, in order to investigate the selectivity of **THTA-GTh** for Hg^{2+} , the control experiments were carried out under the competition conditions. The coexist competition cations

could not induce any interfere for the Hg^{2+} sensing process for **THTA-GTh** (Fig. S17).

The possible sequential ultrasensitive detection mechanism of **THTA-G** for Th^{4+} and Hg^{2+} was investigated carefully by HRMS, FT-IR, XRD, SEM and TEM analysis. In HRMS (Fig. S18), a positive ion peak showed at $m/z = 1234.3651$ [**TH+TA+Th-3H**]⁺, which verified a 1:1 stoichiometric complex formed between **THTA-G** and Th^{4+} . In the FT-IR spectra of **THTA-G** (Fig. S9b), the stretching vibration peaks of N-H and C=O appeared at 3465 cm^{-1} and 1610 cm^{-1} , respectively. After addition of Th^{4+} into the **THTA-G** and the formation of **THTA-GTh**, the stretching vibration peaks of N-H and C=O shifted to 3435 cm^{-1} and 1635 cm^{-1} , respectively, which was attributed to the coordination of Th^{4+} with N-H and C=O groups in **THTA-GTh**. In addition, the **THTA-GTh** didn't have sharp peaks at 2θ from 15 to 30 degrees, and only one sharp peak appeared at 2θ from 10 to 15 degrees (Fig. S10b). These results indicated that the **THTA-G** could combine with Th^{4+} by metal coordination interactions [40-42], and π - π stacking interactions were not involved in **THTA-GTh**. As shown in Fig. 8a, in the concentration-dependent ^1H NMR spectra of **TH**, with increasing concentration of **TH**, the signals of protons H_a , H_b , H_c , H_d and H_e on **TH** all showed distinct shifted downfield and these signal peaks became broad at high concentration, which confirmed that gelator **TH** could assemble to high-molecular-weight aggregates via hydrogen bond interactions. After addition of Hg^{2+} to **THTA**, the signals of protons H_a and H_d almost no shifted, meanwhile, the signals of protons H_c and H_e on **TH**, and H_3 and H_4 on **TA** all shifted downfield (Fig. 8b). To our surprise, for the complex of **THTA-GTh** and Hg^{2+} , the stretching vibration peaks of N-H and C=O shifted to 3459 cm^{-1} and 1617 cm^{-1} respectively (Fig. S9b), which indicated the hydrogen bonds were formed again. Meanwhile, the d-spacings of 4.13 \AA and 3.17 \AA at $2\theta = 21.49^\circ$ and 28.17° appeared (Fig. S10b). These results confirmed that Hg^{2+} didn't interact with N-H and C=O groups, but formed cation- π interactions with the **THTA-GTh** [43,44]. Moreover, the 1:3 stoichiometric complex between **THTA-G** and Hg^{2+} was confirmed by HRMS (Fig. S19). However, after Hg^{2+} was added into the **THTA-GTh**, we didn't find Th^{4+}

participate in the reaction. Therefore, after addition of Hg^{2+} into the **THTA-GTh**, Th^{4+} no longer interacts with the gel.

Fig. 8.

In SEM (Fig. S11), the **THTA-GTh** shows tire-shaped structure, but compared with the **THTA-G**, the distance between layer and layer of tire is wider. After addition of Hg^{2+} into the **THTA-GTh**, the micromorphology also shows tire-shaped tightly stacking structure. In TEM, for **THTA-GTh**, the distance between layer and layer of tire structure is about 150 nm (Fig. S12b). After adding Hg^{2+} to the **THTA-GTh**, the distance between layer and layer of tire is about 57 nm (Fig. S12c). According to aforementioned, Th^{4+} could induce the **THTA-G** to carry out supramolecular aggregates through metal-ligand coordination, leading to the **THTA-GTh** showed distinct green AIE effect. Clearly, this fluorescent enhancement process attributing to Th^{4+} tuned aggregation induced emission. In addition, Hg^{2+} has high ionic strength [45], which is easy to induce the π electrons on benzene ring groups of **TH** and **TA** transfer to Hg^{2+} and act as cation- π interactions, so that Hg^{2+} could be identified through cation- π interactions. Therefore, Hg^{2+} could form stable cation- π interactions with the **THTA-GTh** [46], and then the fluorescence of **THTA-GTh** was induced to weaken again. These results cause the selectivity response of **THTA-GTh** for Hg^{2+} over other metal ions.

As shown in Fig. S20, there arise five broad absorption bands around 275 nm in the UV-vis spectra of **TH**, **TA**, **THTA-G**, **THTA-GTh** and **THTA-GTh** with analyte ions. Compared with the absorbance of **TH** and **TA**, the absorbance of **THTA-G** was obviously decreased, which indicated that the **TH** and **TA** could assemble into aggregates through intermolecular hydrogen bonding [47]. Meanwhile, due to aggregation, the emission of **THTA-G** in the gel state was weak significantly. However, after addition of Th^{4+} into the **THTA-G**, the Th^{4+} could restriction of intramolecular motions (RIM) in the aggregation state, and makes the absorbance of **THTA-GTh** increase again. In addition, the characteristic absorption presented a slight red shift and broadening with increasing Hg^{2+} to the **THTA-GTh**, as well as the absorbance of complex was also decreased, suggesting the Th^{4+} could combine with the aromatic moieties of **TH** and **TA** molecules via cation- π interactions [48].

Therefore, the **THTA-G** could carry out sequential ultrasensitive detection of Th^{4+} and Hg^{2+} through a novel mechanism (Scheme 2b). Based on sequential ultrasensitive detection of **THTA-G** to Th^{4+} and Hg^{2+} , a cations-controlled fluorescence response switch was prepared, and the switching performance could be repeated at least four successive cycles with little fluorescent efficiency loss (Fig. S21).

In order to investigate the adsorption rates of **THTA-G** for Th^{4+} and **THTA-GTh** for Hg^{2+} , the xerogels sample of **THTA-G** (0.001 g) and **THTA-GTh** (0.001 g) were placed in dilute aqueous solution of Th^{4+} (5 mL, $c = 1 \times 10^{-4}$ mol/L) and Hg^{2+} (5 mL, $c = 1 \times 10^{-4}$ mol/L), respectively. After the two mixtures were stirred at room temperature for 20 h, the precipitates were separated by centrifugation (1000r/min, 10 min). Then, the supernatant was analysed by inductively coupled plasma (ICP). As a result, the adsorption rates of **THTA-G** for Th^{4+} and **THTA-GTh** for Hg^{2+} are up to 99.82% and 99.95%, respectively (Table 1). These results indicated that the xerogels of **THTA-G** and **THTA-GTh** have nice separation properties for Th^{4+} and Hg^{2+} in aqueous solution, respectively.

Table 2.

Fig. 9.

A gel film based on the **THTA-G** was prepared by loading **THTA-G** on a clean glass surface. Upon addition of Th^{4+} , the fluorescence of the gel film was changed from weak to strong green. However, after Hg^{2+} was added, the fluorescence of the gel film weakens again (Fig. 9). Therefore, the gel film based on **THTA-G** is suitable for immediate visualization of Th^{4+} and Hg^{2+} by a very simple practical method that should be applicable for rapid on-site testing.

4. Conclusion

In conclusion, a novel strategy for sequential ultrasensitive detection of Th^{4+} and Hg^{2+} based on “ Th^{4+} tuned aggregation-induced emission” mechanism was proposed. Two easy-to-make tripodal gelators **TH** and **TA** could assemble into a stable supramolecular polymer hydrogel **THTA-G** by intermolecular interactions in aqueous media. Interestingly, Th^{4+} could tune the **THTA-G** shows strong green AIE effect with ultrasensitive response to Th^{4+} . Meanwhile, the obtained metallogel **THTA-GTh**

shows ultrasensitive stimuli-responsive to Hg^{2+} . The detection limits of **THTA-G** and **THTA-GTh** for Th^{4+} and Hg^{2+} are 8.61×10^{-11} mol/L and 1.08×10^{-11} mol/L, respectively. Moreover, the separate rates of **THTA-G** and **THTA-GTh** for Th^{4+} and Hg^{2+} reached up to 99.82% and 99.95%, respectively. Therefore, the **THTA-G** and **THTA-GTh** have good potential for practical application in ions detection and separation, and smart light-emitting materials. This work enriches the AIE effect and provides new thinking for the smart materials design.

Declaration of Competing Interest

There are no conflicts to declare.

Acknowledgements

This work was supported by the National Natural Science Foundation of China (Nos. 21661028; 21662031; 21574104), the Program for Changjiang Scholars and Innovative Research Team in University of Ministry of Education of China (IRT 15R56).

References

- [1] A. Pankajakshan, D. Kuznetsov, S. Mandal, Ultrasensitive detection of Hg(II) ions in aqueous medium using zinc-based metal-organic framework, *Inorg. Chem.* 58 (2019) 1377-1381.
- [2] Y. Yang, J. Zhu, J. Zhao, G.J. Weng, J.J. Li, J.W. Zhao, Growth of spherical gold satellites on the surface of Au@Ag@SiO₂ core-shell nanostructures used for an ultrasensitive SERS immunoassay of alpha-fetoprotein, *ACS Appl. Mater. Interfaces* 11 (2019) 3617-3626.
- [3] P. Zhang, J. Crow, D. Lella, X. Zhou, G. Samuel, A.K. Godwin, Y. Zeng, Ultrasensitive quantification of tumor mRNAs in extracellular vesicles with an integrated microfluidic digital analysis chip, *Lab Chip.* 18 (2018) 3790-3801.
- [4] M. Liu, H. Zhao, X. Quan, S. Chen, H. Yu, Signal amplification via cation exchange reaction: an example in the ratiometric fluorescence probe for

- ultrasensitive and selective sensing of Cu(II), *Chem. Commun.* 46 (2010) 1144-1146.
- [5] A. Gupta, A. Chaudhary, P. Mehta, C. Dwivedi, S. Khan, N.C. Verma, C.K. Nandi, Nitrogen doped thiol functionalized carbon dots for ultrasensitive Hg (II) detection, *Chem. Commun.* 51 (2015) 10750-10753.
- [6] Z. Wen, W. Liang, Y. Zhuo, C. Xiong, Y. Zheng, R. Yuan, Y. Chai, An efficient target-intermediate recycling amplification strategy for ultrasensitive fluorescent assay of intracellular lead ion, *Chem. Commun.* 53 (2017) 7525-7528.
- [7] D. Fapyane, J.S. Nielsen, E.E. Ferapontova, Electrochemical enzyme-linked sandwich assay with a cellulase label for ultrasensitive analysis of synthetic DNA and cell-isolated RNA, *ACS Sens.* 3 (2018) 2104-2111.
- [8] Z. Wang, A.T. Brown, K. Tan, Y.J. Chabal, K.J. Balkus, Jr. Selective extraction of thorium from rare earth elements using wrinkled mesoporous carbon, *J. Am. Chem. Soc.* 140 (2018) 14735-14739.
- [9] E.E. Hardy, K.M. Wyss, J.D. Gorden, I.R. Ariyaratna, E. Miliordos, A.E.V. Gorden, Th(IV) and Ce(IV) naphthylsalophen sandwich complexes: characterization of unusual thorium fluorescence in solution and solid-state, *Chem. Commun.* 53 (2017) 11984-11987.
- [10] L.S. Walekar, P. Hu, H.V. Molamahmood, M. Long, FRET based integrated pyrene-AgNPs system for detection of Hg (II) and pyrene dimer: Applications to environmental analysis, *Spectrochim. Acta A* 198 (2018) 168-176.
- [11] Z. Ruan, Y. Shan, Y. Gong, C. Wang, F. Ye, Y. Qiu, Z. Liang, Z. Li, Novel AIE-active ratiometric fluorescent probes for mercury(II) based on the Hg²⁺-promoted deprotection of thioketal, and good mechanochromic properties, *J. Mater. Chem.* 6 (2018) 773-780.
- [12] J. Luo, Z. Xie, J.W.Y. Lam, L. Cheng, H. Chen, C. Qiu, H.S. Kwok, X. Zhan, Y. Liu, D. Zhu, B.Z. Tang, Aggregation-induced emission of 1-methyl-1,2,3,4,5-pentaphenylsilole, *Chem. Commun.* (2001) 1740-1741.
- [13] W.K. Tsai, C.I. Wang, C.H. Liao, C.N. Yao, T.J. Kuo, M.H. Liu, C.P. Hsu, S.Y. Lin, C.Y. Wu, J.R. Pyle, J. Chen, Y.H. Chan, Molecular design of near-infrared

- fluorescent Pdots for tumor targeting: aggregation-induced emission versus anti-aggregation-caused quenching, *Chem. Sci.* 10 (2019) 198-207.
- [14] J. Mei, N.L.C. Leung, R.T.K. Kwok, J.W.Y. Lam, B.Z. Tang, Aggregation-induced emission: together we shine, united we soar! *Chem. Rev.* 115 (2015) 11718-11940.
- [15] J.N. Zhang, H. Kang, N. Li, S.M. Zhou, H.M. Sun, S.W. Yin, N. Zhao, B.Z. Tang, Organic solid fluorophores regulated by subtle structure modification: color-tunable and aggregation-induced emission, *Chem. Sci.* 8 (2017) 577-582.
- [16] D. Dai, Z. Li, J. Yang, C. Wang, J.R. Wu, Y. Wang, D. Zhang, Y.W. Yang, Supramolecular assembly-induced emission enhancement for efficient mercury(II) detection and removal, *J. Am. Chem. Soc.* 141 (2019) 4756-4763.
- [17] L. Shao, J. Sun, B. Hua, F. Huang, An AIEE fluorescent supramolecular cross-linked polymer network based on pillar[5]arene host-guest recognition: construction and application in explosive detection, *Chem. Commun.* 54 (2018) 4866-4869.
- [18] F. Hu, X. Cai, P.N. Manghnani, Kenry, W. Wu, B. Liu, Multicolor monitoring of cellular organelles by single wavelength excitation to visualize the mitophagy process, *Chem. Sci.* 9 (2018) 2756-2761.
- [19] X. Yan, D. Xu, X. Chi, J. Chen, S. Dong, X. Ding, Y. Yu, F. Huang, A multiresponsive, shape-persistent, and elastic supramolecular polymer network gel constructed by orthogonal self-assembly, *Adv. Mater.* 24 (2012) 362-369.
- [20] X. Ma, Z. Zhang, H. Xie, Y. Ma, C. Liu, S. Liu, M. Liu, Emissive intelligent supramolecular gel for highly selective sensing of Al³⁺ and writable soft material, *Chem. Commun.* 54 (2018) 13674-13677.
- [21] S. Seiffert, Origin of nanostructural inhomogeneity in polymer-network gels, *Polym. Chem.* 8 (2017) 4472-4487.
- [22] W. Feng, M. Jin, K. Yang, Y. Pei, Z. Pei, Supramolecular delivery systems based on pillararenes, *Chem. Commun.* 54 (2018) 13626-13640.

- [23] X. Li, J. Han, X. Wang, Y. Zhang, C. Jia, J. Qin, C. Wang, J.R. Wu, W. Fang, Y.W. Yang, A triple-stimuli responsive hormone delivery system equipped with pillararene magnetic nanovalves, *Mater. Chem. Front.* 3 (2019) 103-110.
- [24] Y. Liu, L. Shanguan, H. Wang, D. Xia, B. Shi, A supramolecular polymer network gel with stimuli-responsiveness constructed by orthogonal metal ion coordination and pillar[5]arene-based host-guest recognition, *Polym. Chem.* 8 (2017) 3783-3787.
- [25] H. Yuk, B. Lua, X. Zhao, Hydrogel bioelectronics, *Chem. Soc. Rev.* 48 (2019) 1642-1667.
- [26] L. Voorhaar, R. Hoogenboom, Supramolecular polymer networks: hydrogels and bulk materials, *Chem. Soc. Rev.* 45 (2016) 4013-4031.
- [27] J. Hai, X. Zeng, Y. Zhu, B. Wang, Anions reversibly responsive luminescent nanocellulose hydrogels for cancer spheroids culture and release, *Biomaterials* 194 (2019) 161-170.
- [28] M. Yan, X.B. Liu, Z.Z. Gao, Y.P. Wu, J.L. Hou, H. Wang, D.W. Zhang, Y. Liu, Z.T. Li, A pore-expanded supramolecular organic framework and its enrichment of photosensitizers and catalysts for visible-light-induced hydrogen production, *Org. Chem. Front.* 6 (2019) 1698-1704.
- [29] B. Jiang, L.J. Chen, G.Q. Yin, Y.X. Wang, W. Zheng, L. Xu, H.B. Yang, Multiphase transition of supramolecular metallogels triggered by temperature, *Chem. Commun.* 53 (2017) 172-175.
- [30] Y.M. Zhang, W. Zhu, W.J. Qu, K.P. Zhong, X.P. Chen, H. Yao, T.B. Wei, Q. Lin, Competition of cation- π and exo-wall π - π interactions: a novel approach to achieve ultrasensitive response, *Chem. Commun.* 54 (2018) 4549-4552.
- [31] Q. Lin, G.F. Gong, Y.Q. Fan, Y.Y. Chen, J. Wang, X.W. Guan, J. Liu, Y.M. Zhang, H. Yao, T.B. Wei, Anion induced supramolecular polymerization: a novel approach for the ultrasensitive detection and separation of F^- , *Chem. Commun.* 55 (2019) 3247-3250.
- [32] Y.Q. Fan, J. Liu, Y.Y. Chen, X.W. Guan, J. Wang, H. Yao, Y.M. Zhang, T.B. Wei, Q. Lin, An easy-to-make strong white AIE supramolecular polymer as a

- colour tunable photoluminescence material, *J. Mater. Chem. C* 6 (2018) 13331-13335.
- [33] L. Zong, Y. Xie, C. Wang, J.R. Li, Q. Li, Z. Li, From ACQ to AIE: the suppression of the strong π - π interaction of naphthalene diimide derivatives through the adjustment of their flexible chains, *Chem. Commun.* 52 (2016) 11496-11499.
- [34] B. Fu, J. Huang, D. Bai, Y. Xie, Y. Wang, S. Wang, X. Zhou, Label-free detection of pH based on the i-motif using an aggregation-caused quenching strategy, *Chem. Commun.* 51 (2015) 16960-16963.
- [35] X. Cao, N. Zhao, A. Gao, H. Lv, Y. Jia, R. Wu, Y. Wu, Bis-naphthalimides self-assembly organogel formation and application in detection of *p*-phenylenediamine, *Mat. Sci. Eng. C* 70 (2017) 216-222.
- [36] S. Mondal, K. Ghosh, Anthraquinone derived cholesterol linked imidazole gelator in visual sensing of picric acid, *ChemistrySelect* 2 (2017) 4800-4806.
- [37] S. Wang, B. Lin, L. Chen, N. Li, J. Xu, J. Wang, Y. Yang, Y. Qi, Y. She, X. Shen, X. Xiao, Branch-migration based fluorescent probe for highly sensitive detection of mercury, *Anal. Chem.* 90 (2018) 11764-11769.
- [38] Z. Yang, Z. Chi, Z. Mao, Y. Zhang, S. Liu, J. Zhao, M.P. Aldred, Z. Chi, Recent advances in mechano-responsive luminescence of tetraphenylethylene derivatives with aggregation-induced emission properties, *Mater. Chem. Front.* 2 (2018) 861-890.
- [39] A.C.B. Rodrigues, J. Pina, W. Dong, M. Forster, U. Scherf, J.S. Seixas de Melo, Aggregation-induced emission in phenothiazine-TPE and -TPAN polymers, *Macromolecules* 51 (2018) 8501-8512.
- [40] L. Shao, J. Yang B. Hua, Dual-responsive cross-linked supramolecular polymer network gel: hierarchical supramolecular self-assembly driven by pillararene-based molecular recognition and metal-ligand interaction, *Polym. Chem.* 9 (2018) 1293-1297.

- [41] H. Ding, X. Liang, X.N. Zhang, Z.L. Wu, Z. Li, G. Sun, Tough supramolecular hydrogels with excellent self-recovery behavior mediated by metal-coordination interaction, *Polymer* 171 (2019) 201-210.
- [42] L. Lu, T. Tian, S. Wu, T. Xiang, S. Zhou, A pH-induced self-healable shape memory hydrogel with metal-coordination cross-links, *Polym. Chem.* 10 (2019) 1920-1929.
- [43] S. Yamada, Cation- π interactions in organic synthesis, *Chem. Rev.* 118 (2018) 11353-11432.
- [44] S.C. Sha, S. Teyrulnikov, M. Li, B. Hu, Y. Fu, M.C. Kozlowski, P.J. Walsh, Cation- π interactions in the benzylic arylation of toluenes with bimetallic catalysts, *J. Am. Chem. Soc.* 140 (2018) 12415-12423.
- [45] A.K. Pearson, P. Kao, A.P. O'Mullane, A.I. Bhatt, Investigating the effect of ionic strength on the suppression of dendrite formation during metal electrodeposition, *Phys. Chem. Chem. Phys.* 19 (2017) 14745-14760.
- [46] Q. Lin, P.P. Mao, Y.Q. Fan, L. Liu, J. Liu, Y.M. Zhang, H. Yao, T.B. Wei, A novel supramolecular polymer gel based on naphthalimide functionalized-pillar[5]arene for the fluorescence detection of Hg^{2+} and I^- and recyclable removal of Hg^{2+} via cation- π interactions, *Soft Matter*, 13 (2017) 7085-7089.
- [47] Q. Li, R. Li, H. Lan, Y. Lu, Y. Li, S. Xiao, T. Yi, Halogen Effect on Non-Conventional Organogel Assisted by Balanced π - π Interaction, *ChemistrySelect* 2 (2017) 5421-5426.
- [48] A. Hirano, K. Iwashita, T. Ura, S. Sakuraba, K. Shiraki, T. Arakawa, T. Kameda, The binding affinity of uncharged aromatic solutes for negatively charged resins is enhanced by cations via cation- π interactions: The case of sodium ion and arginine, *J. Chromatogr. A* 1595 (2019) 97-107.

Author statement

You-Ming Zhang: Conceptualization, Funding acquisition, Validation.

Wei Zhu: Software, Formal analysis, Data Curation, Writing - Original Draft.

Qi Zhao: Data Curation.

Wen-Juan Qu: Data Curation.

Hong Yao: Supervision, Project administration.

Tai-Bao Wei: Funding acquisition, Methodology, Visualization.

Qi Lin: Funding acquisition, Investigation, Writing - Review & Editing.

Declaration of interests

The authors declare that they have no known competing financial interests or personal relationships that could have appeared to influence the work reported in this paper.

The authors declare the following financial interests/personal relationships which may be considered as potential competing interests:

Journal Pre

Figure Captions

Scheme 1. Synthesis of compounds **TA** and **TH**.

Fig. 1. Gelation property of supramolecular polymer hydrogel **THTA-G** (3.3 wt%, 10 mg/ml = 1.0%) in DMSO/H₂O (3.3:6.7, v/v) binary-solution.

Fig. 2. Temperature-dependent fluorescence spectra of (a) **THTA-G** and (b) **THTA-GTh** during the gelation process ($\lambda_{\text{ex}} = 370$ nm).

Fig. 3. The laser scanning confocal microscopy (LSCM) images of (a) **THTA-G**; (b) **THTA-GTh**; (c) **THTA-GTh+Hg²⁺**.

Fig. 4. (a) Partial ¹H NMR (400 MHz, DMSO-*d*₆) spectra of **THTA**, from bottom to top: 2.82×10^{-2} mol/L **TH**; 3.65×10^{-2} mol/L **TA**; 2.82×10^{-2} mol/L **TH** and 5.64×10^{-2} mol/L **TA**. (b) Partial concentration-dependent ¹H NMR spectra (400 MHz, DMSO-*d*₆) of **THTA**, from bottom to top: 2.82×10^{-2} mol/L **TH**; 2.74×10^{-2} mol/L **TA**; 1.05×10^{-1} mol/L **TH** and 8.22×10^{-1} mol/L **TA**.

Scheme 2. Schematic illustration of the sequential ultrasensitive detection and separation of Th⁴⁺ and Hg²⁺ from aqueous solution based on the Th⁴⁺ tuned aggregation induced emission mechanism.

Fig. 5. (a) Fluorescence response properties of **THTA-G** to different metal ions. (b) Fluorescence response properties of **THTA-GTh** to different metal ions.

Fig. 6. Fluorescence spectra of (a) **THTA-G** and **THTA-GTh**; (b) **THTA-GTh** and **THTA-GTh+Hg²⁺**. Fluorescence spectra of (c) **THTA-G** with increasing amounts of Th⁴⁺; (d) **THTA-GTh** with increasing amounts of Hg²⁺ ($\lambda_{\text{ex}} = 370$ nm).

Fig. 7. The detection limits of (a) **THTA-G** for Th⁴⁺; and (b) **THTA-GTh** for Hg²⁺.

Fig. 8. (a) Partial concentration-dependent ¹H NMR (400 MHz, DMSO-*d*₆) spectra of **TH**, from bottom to top: 2.47×10^{-2} mol/L **TH**; 1.76×10^{-1} mol/L **TH**. (b) Partial ¹H NMR spectra (400 MHz, DMSO-*d*₆) of **THTA** with various equivalents of Hg²⁺, from

bottom to top: 2.82×10^{-2} mol/L **TH**; 2.74×10^{-2} mol/L **TA**; 1.0 equivalent of Hg^{2+} ; 2.0 equivalents of Hg^{2+} .

Fig. 9. Photographs of **THTA-G**-based films fluorescently (365 nm UV-lamp) sense Th^{4+} and Hg^{2+} .

Table 1. Adsorption rates of **THTA-G** for Th^{4+} and **THTA-GTh** for Hg^{2+} .

Ion	Initial concentration (mol/L)	Residual concentration (mol/L)	Adsorption rate%
Th^{4+}	1.0×10^{-4}	1.80×10^{-7}	99.82%
Hg^{2+}	1.0×10^{-4}	5.0×10^{-8}	99.95%

Graphical abstract

A novel strategy, Th⁴⁺ tuned aggregation-induced emission was developed successfully. Based on this strategy, sequential ultrasensitive detection and separation of Th⁴⁺ and Hg²⁺ were achieved.

Journal Pre-proof

Highlights

1. A novel strategy for sequential ultrasensitive detection of Th^{4+} and Hg^{2+} .
2. Stable supramolecular polymer hydrogel **THTA-G** was constructed.
3. Th^{4+} could tune the hydrogel **THTA-G** generation of AIE effect.
4. The xerogels of **THTA-G** and **THTA-GTh** could separation of Th^{4+} and Hg^{2+} .
5. **THTA-G** could act as a novel smart light-emitting material.

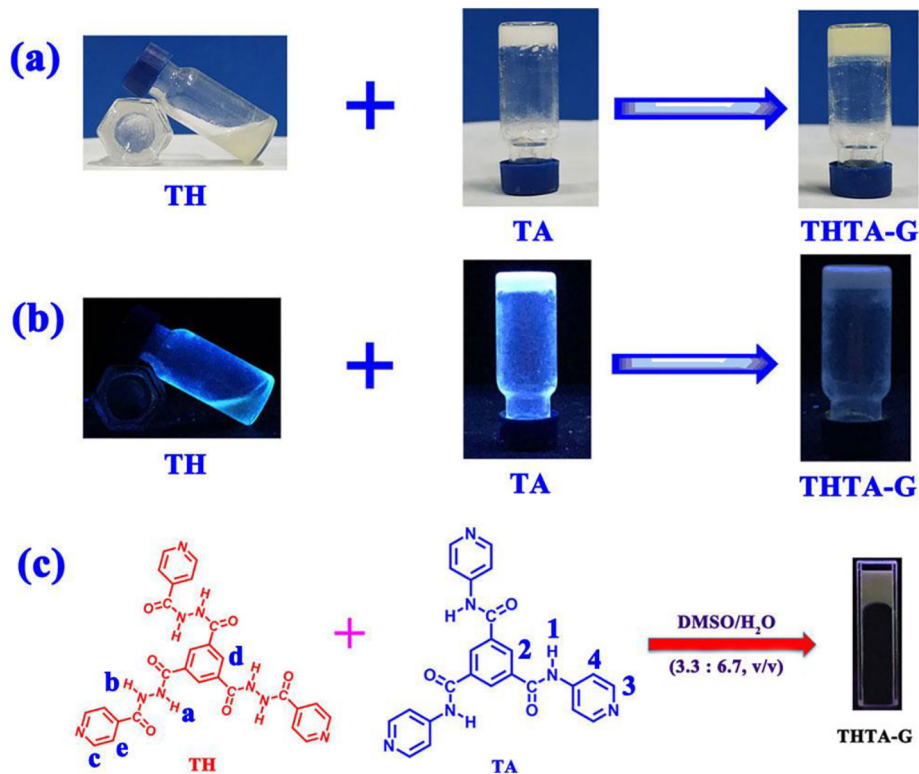


Figure 1

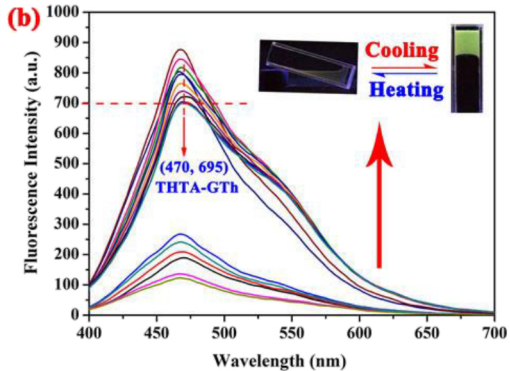
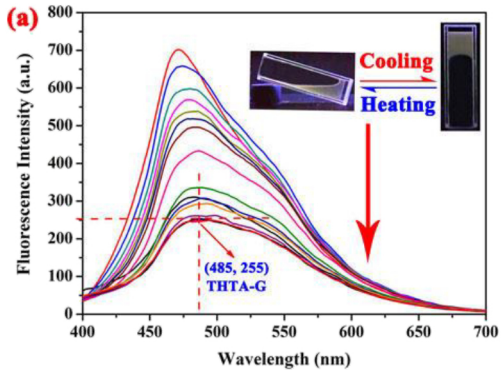


Figure 2

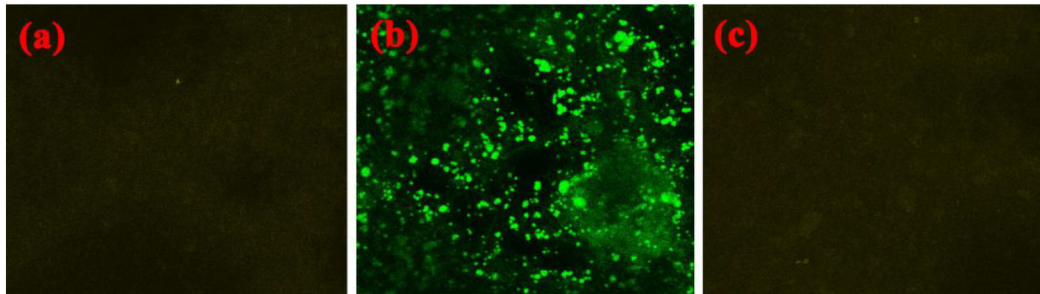


Figure 3

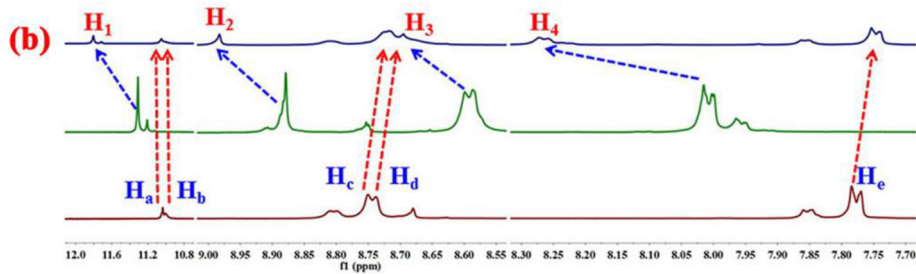
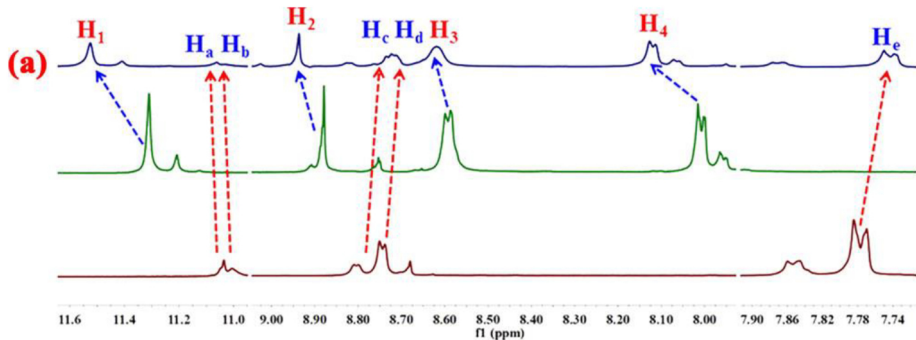


Figure 4

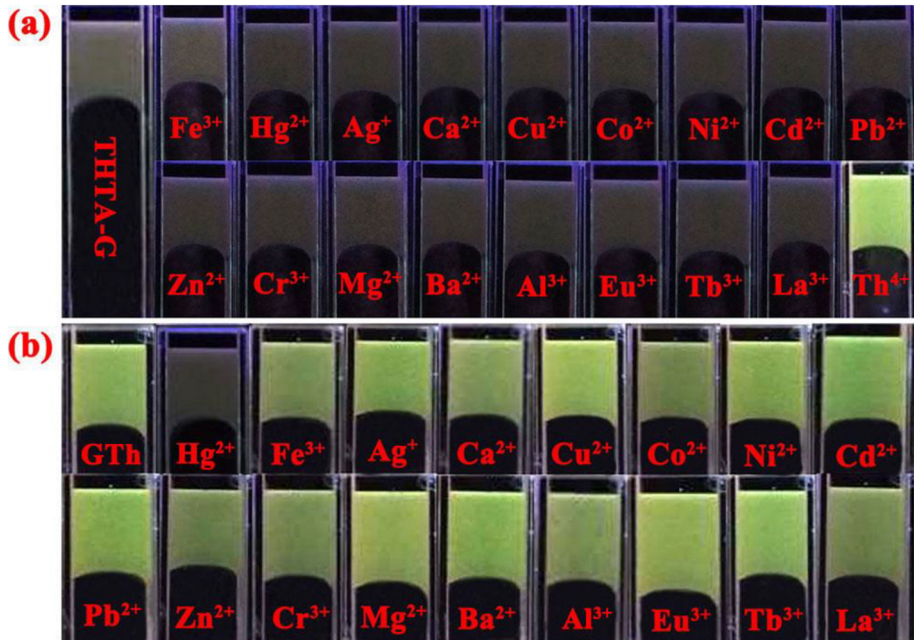


Figure 5

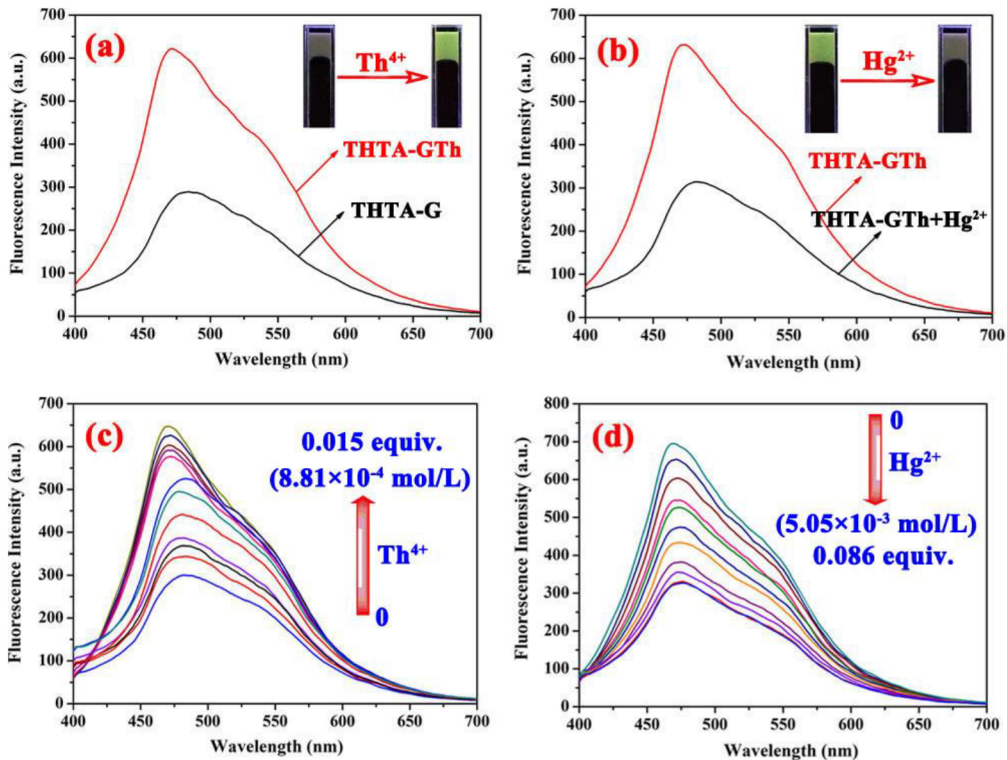


Figure 6

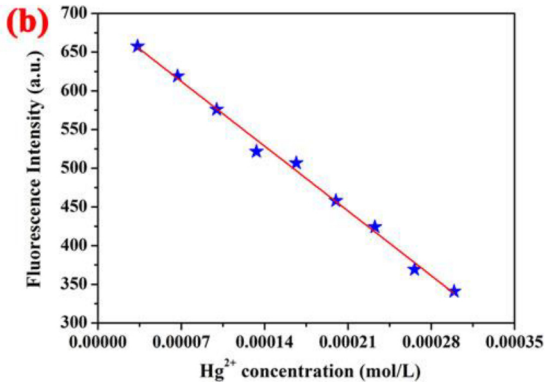
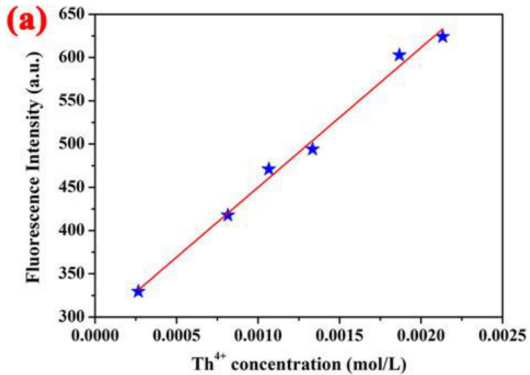


Figure 7

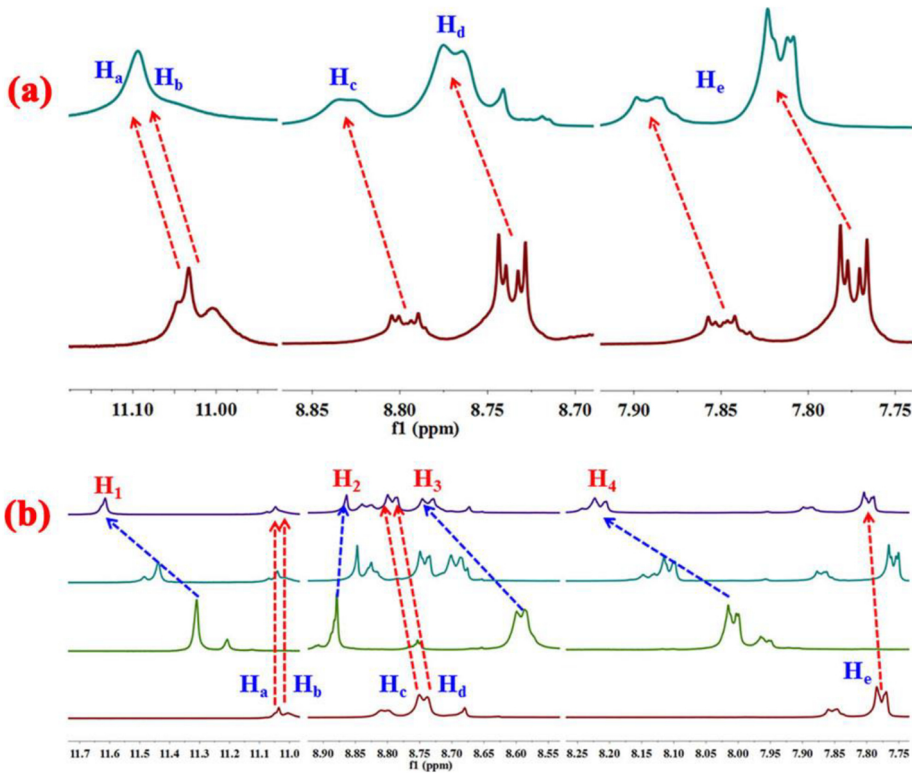


Figure 8

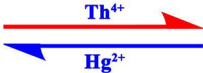


Figure 9